

Many-body localization transition in quantum annealing of graph coloring

Kazue Kudo^{1,*}

¹*Department of Computer Science, Ochanomizu University, Tokyo 112-8610, Japan*

(Dated: December 20, 2024)

The many-body localization (MBL) transition is a dynamical phase transition where the interplay between many-body interaction and disorder plays an essential role. The model used for quantum annealing of graph coloring has an analogy with a disordered spin chain. In the model, disorder corresponds to effective random fields which increases in a quantum annealing process. Some measures of entanglement, which is essential to quantum computation, show the evidence of the MBL transition in quantum annealing.

I. INTRODUCTION

Entanglement plays an essential role for speedup in quantum computation [1–3]. However, the role of entanglement in adiabatic quantum computation and quantum annealing (QA) is currently unclear [4–7]. QA is well known as a quantum-mechanical approach for combinatorial optimization problems [8–16]. In a QA framework, the total Hamiltonian consists of a problem Hamiltonian H_p and a driving Hamiltonian H_d :

$$H(s) = sH_p + (1 - s)H_d, \quad (1)$$

where s is a time dependent parameter. The QA process starts with the ground state of H_d at $s = 0$ and ends at $s = 1$. If the process is adiabatic, the solution of an optimization problem, which is the ground state of H_p , is obtained as the ground state of the total Hamiltonian in the end. The computational efficiency of QA depends on the energy gap between the ground and the first-excited states. However, the connection between the energy gap and entanglement is not well understood.

Entanglement also characterizes many-body localization (MBL) in quantum systems where the interplay between disorder and many-body interaction is important. In the MBL phase, where disorder is relatively strong, quantum dynamics is nonergodic and breaks the eigenstate thermalization hypothesis (ETH) [17–19]. While many-body eigenstates in the ETH phase have a large amount (volume law) of entanglement, MBL eigenstates have low (area-law) entanglement. Entanglement entropy (EE) is often employed to characterize the MBL transition [20–29]. In a disordered quantum spin chain, for instance, the standard deviation of the half-chain EE has a peak at around the MBL transition [27–30].

In this paper, we explore the evidence of the MBL transition in QA by means of entanglement. While MBL occurs in systems with disordered fields, the system considered in QA usually has no external random fields. However, a spin can feel inhomogeneous fields from neighboring spins, even if random fields are not applied externally. For example, the total Hamiltonian for the constrained

quantum annealing (CQA) of graph coloring is analogous to an ensemble of spin chains with disordered fields [31]. In CQA approaches, the driving Hamiltonian is chosen so that it commutes with constraint operators but not with the problem Hamiltonian [31–33]. In the CQA of graph coloring, the driving Hamiltonian consists of independent spin chains. This implies that the system is almost independent spin chains interacting weakly with other chains in the early stage of the CQA. In the late stage, since inter-chain interaction increases with time, spins are affected by effective fields arising from neighboring chains. These effective fields can cause the MBL transition. To examine the MBL transition, we investigate quantum dynamics and entanglement evolution using real-time quantum simulations. Several kinds of measures of entanglement suggest that the MBL transition occurs in the CQA process of graph coloring.

The rest of the paper is organized as follows. In Sec. II, the model for the CQA of graph coloring is introduced, and numerical methods are outlined. In Sec. III, time dependence of effective fields is illustrated. Results on EE and concurrence, which are measures of entanglement, are presented in Secs. IV and V, respectively. Discussion and conclusions are given in Sec. VI.

II. MODELS AND METHODS

We here focus on the CQA of graph coloring whose model was introduced in Ref. [31]. Graph coloring is coloring the nodes of a graph such that no pair of nodes connected by an edge has the same color. For coloring a graph $G = (V, E)$ with q available colors, the classical Hamiltonian is given by

$$H_{\text{cl}} = \sum_{(ij) \in E} \sum_{a=1}^q \frac{S_{i,a} + 1}{2} \frac{S_{j,a} + 1}{2}, \quad (2)$$

where i and j represent nodes $V = \{1, \dots, N\}$, and $(ij) \in E$ denotes the edge connecting the pair of nodes $i, j \in V$. If node i is colored a , $S_{i,a} = 1$; otherwise, $S_{i,a} = -1$. Thus, Eq. (2) counts the number of edges that connect nodes with the same color. The quantum version of Eq. (2) is the problem Hamiltonian, which is

* kudo@is.ocha.ac.jp

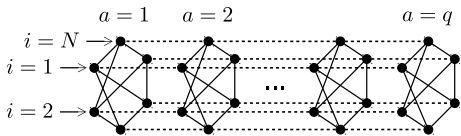


FIG. 1. Schematic of the model [31]. The solid and broken lines correspond to the problem Hamiltonian (3) and the driving Hamiltonian (4), respectively.

given by

$$H_p = J \sum_{(ij) \in E} \sum_{a=1}^q \sigma_{i,a}^z \sigma_{j,a}^z, \quad (3)$$

where $\sigma_{i,a}^z$ denotes the Pauli matrix of the z component, and J has a unit of energy ($J = 1$ in the simulations below). Since one node must have only one color, we need the constraint that $\langle \sum_{a=1}^q \sigma_{i,a}^z \rangle = 2 - q$. In standard QA approaches, the penalty term to satisfy the constraint is often incorporated into the problem Hamiltonian [34–38]. In the CQA approach, however, we choose the driver Hamiltonian so that the constraint is satisfied consistently, instead of adding a penalty term. Here, we give the driving Hamiltonian for this problem as

$$H_d = -J \sum_{i=1}^N \sum_{a=1}^q (\sigma_{i,a}^x \sigma_{i,a+1}^x + \sigma_{i,a}^y \sigma_{i,a+1}^y), \quad (4)$$

where periodic boundary conditions are imposed for index a . Since the total Hamiltonian, which consists of H_p and H_d , is a kind of XXZ model, the magnetization $\langle \sum_{a=1}^q \sigma_{i,a}^z \rangle$ is conserved for each i .

The model is a kind of an ensemble of tight-binding chains. In Fig. 1, which is a schematic of the model, each broken line corresponds to a tight-binding chain. Since there is only one up-spin in each chain, no interaction among up-spins exists in a tight-binding chain. However, as represented in Fig. 1, each site of a chain (a broken line) interacts with the corresponding site of neighboring chains through the problem Hamiltonian (solid lines). This gives an interpretation that a tight-binding chain is affected by effective local fields which arise from the spins in its neighboring chains.

The advantage of the CQA approach is not only that constraints are consistently satisfied without penalty terms but also that the dimension of the Hilbert space is considerably reduced. The dimension reduction is essential for simulations based on real-time Schrödinger evolution. In a standard approach to perform real-time quantum simulations, $2^q N$ dimensions are required for coloring a graph with N nodes with q colors. However, in the CQA approach described above, the required dimension is reduced to only q^N .

To perform the CQA based on real-time quantum simulations, we deal with only the subspace that satisfies the constraint $\langle \sum_{a=1}^q \sigma_{i,a}^z \rangle = 2 - q$. The initial state is taken as the lowest-energy state of H_d in the subspace.

Although this initial state is not the global ground state, the state can be prepared in the whole Hilbert space of the system by adding additional Zeeman term with an appropriate magnetic field [33]. In the following sections, we refer to the lowest energy state in the subspace as the ground state. Time evolution is calculated by solving the time-dependent Schrödinger equation by the fourth Runge-Kutta method. The annealing schedule is taken as $s(t) = t/\tau$, where t is time and τ is the final time, so that $s(0) = 0$ and $s(\tau) = 1$. Time is measured in units of \hbar/J .

III. EFFECTIVE FIELDS

When $s > 0$, spins feel effective local fields caused by the interaction between neighboring nodes in a given graph. Note that the problem Hamiltonian (3) can be rewritten as

$$H_p = \sum_{i=1}^N \sum_{a=1}^q \left(\sum_{j=1}^N J_{ij} \sigma_{j,a}^z \right) \sigma_{i,a}^z, \quad (5)$$

where $J_{ij} = J/2$ for $(ij) \in E$, otherwise 0. The effective field, which is time dependent, is defined as

$$h^{\text{eff}} = \langle \hat{h}_{i,a}^{\text{eff}}(s) \rangle \equiv \langle \Psi(s) | \hat{h}_{i,a}^{\text{eff}}(s) | \Psi(s) \rangle, \quad (6)$$

where $|\Psi(s)\rangle$ is the wavefunction at s and

$$\hat{h}_{i,a}^{\text{eff}}(s) = s \sum_{j=1}^N J_{ij} \sigma_{j,a}^z. \quad (7)$$

Similarly, the fluctuation of the effective field is defined as

$$\Delta^{\text{eff}} \equiv \sqrt{\langle (\hat{h}_{i,a}^{\text{eff}}(s))^2 \rangle - \langle \hat{h}_{i,a}^{\text{eff}}(s) \rangle^2}. \quad (8)$$

Considering regular random graphs with connectivity c , the effective field at $s = 1$ is estimated as

$$\langle \hat{h}_{i,a}^{\text{eff}} \rangle = \frac{cJ}{2} \left(\frac{1}{q} - \frac{q-1}{q} \right) = -\frac{cJ(q-2)}{2q}. \quad (9)$$

Similarly, we have $\langle (\hat{h}_{i,a}^{\text{eff}})^2 \rangle = (cJ^2/4)[1 + (c-1)(q-2)^2/q^2]$. Thus, the fluctuation at $s = 1$ is estimated as

$$\Delta^{\text{eff}} = \frac{J}{2} \sqrt{c \left[1 - (q-2)^2/q^2 \right]}. \quad (10)$$

Numerical simulations (Fig. 2) demonstrate that both the effective field h^{eff} and its fluctuation Δ^{eff} changes linearly with s . Although the data in Fig. 2 are only for $i = a = 1$, their behavior is independent of i and a . The simulations are for $N = 6$, $q = 4$, $c = 3$, and $\tau = 20$, the data are averaged over 500 realizations of random regular graphs. The annealing process for this parameter setting is almost adiabatic [31]. Substituting $J = 1$, $c = 3$, and $q = 4$ into Eqs. (9) and (10), we have $h^{\text{eff}} = -3/4$ and $\Delta^{\text{eff}} = 3/4$. Numerical result of h^{eff} coincides with the estimated value, although that of Δ^{eff} is a little larger than the estimated value.

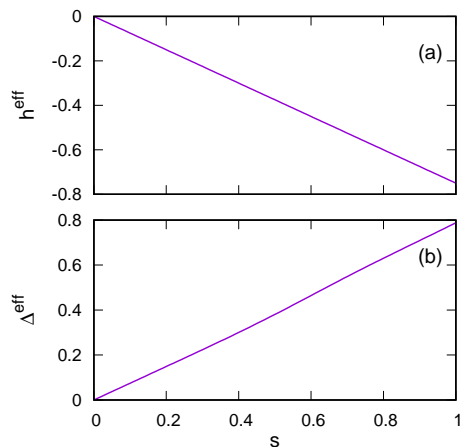


FIG. 2. Time evolution of the effective field h^{eff} and its fluctuation Δ^{eff} for $c = 3$ and $q = 4$.

IV. ENTANGLEMENT ENTROPY

Entanglement entropy (EE) is often used as an entanglement measure, which is defined by

$$S_E = -\text{Tr}(\rho_A \ln \rho_A), \quad (11)$$

where ρ_A is the reduced density matrix of subsystem A . The behavior of EE depends on how to choose the subsystem. We here examine two kinds of EE: half-chain EE and one-chain EE. The half-chain EE is often used in the case of a one-dimensional spin chain. In our system, subsystem A is half of the system, i.e., spins with $a = 1, \dots, N/2$. For the one-chain EE, subsystem A is taken as the chain (a broken line in Fig. 1) of $i = 1$.

In this section, we examine time dependence of the two kinds of EE divided by the Page value [29, 39, 40], which is defined by

$$S_T = \sum_{k=n+1}^{mn} \frac{1}{k} - \frac{m-1}{2n}. \quad (12)$$

While $m = n = q^{N/2}$ for the half-chain EE, $m = q$ and $n = q^{N-1}$ for the one-chain EE. In the simulations below, the number of color and the final time are taken as $q = 4$ and $\tau = 20$, respectively. The average and standard deviation of EE are calculated from the data of 500 realizations of regular random graphs with connectivity c and the number of nodes N .

The time dependence of the half-chain EE is illustrated in Fig. 3. The average half-chain EE increases with time monotonically. Roughly speaking, the larger the connectivity c of random graphs, the larger the half-chain EE. The standard deviation of the half-chain EE tends to increase with time, although no systematic dependence on c or N appears.

By contrast, clear peaks appear in the standard deviation of the one-chain EE, as shown in Fig. 4, although the time dependence of the average one-chain EE looks

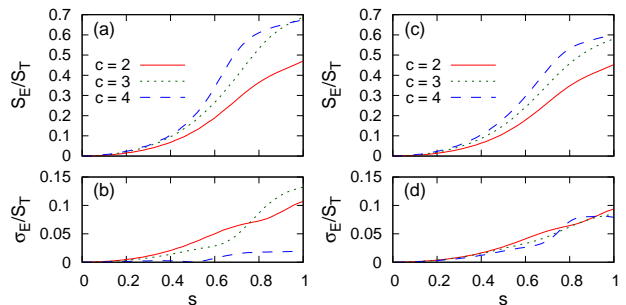


FIG. 3. Time dependence of the average S_E [(a) and (c)] and the standard deviation σ_E [(b) and (d)] of the half-chain EE divided by the Page value S_T for several values of connectivity c of regular random graphs. The number of nodes are $N = 6$ [(a) and (b)] and $N = 8$ [(c) and (d)].

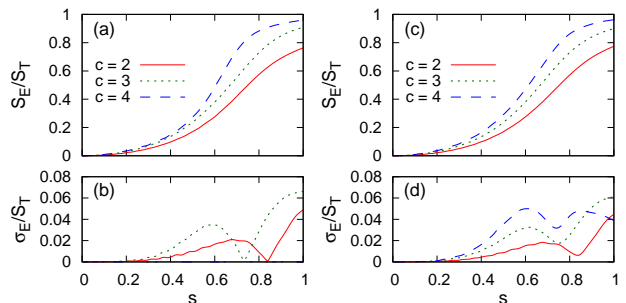


FIG. 4. Time dependence of the average S_E [(a) and (c)] and the standard deviation σ_E [(b) and (d)] of the one-chain EE divided by the Page value S_T for several values of connectivity c of regular random graphs. The number of nodes are $N = 6$ [(a) and (b)] and $N = 8$ [(c) and (d)].

similar to that of the half-chain EE. These peaks indicate the MBL transition. Actually, the peak of the standard deviation of EE corresponds to the MBL transition in a disordered quantum spin chain [27–30]. The standard deviation σ_E also shows system-size dependence: The height of the peak is lower and the trough after the peak is shallower for $N = 8$ than $N = 6$. In Fig. 4(b), σ_E for $c = 4$ is almost 0 because $c = 4$ is too large to produce fluctuation for $N = 6$. We will discuss the second peaks of σ_E later in Sec. VI.

V. CONCURRENCE

We here employ concurrence as another measure of entanglement. Since concurrence is defined for two spins, it is useful for comparison of entanglement in different dimensional systems. The concurrence $C_{i,j}$ in spins i and j is defined from the eigenvalues of the matrix $\rho_{ij}\tilde{\rho}_{ij}$, where ρ_{ij} is the reduced density matrix, and $\tilde{\rho}_{ij} = \sigma^y \otimes \sigma^y \rho_{ij}^* \sigma^y \otimes \sigma^y$. Suppose that the eigenvalues are $\lambda_1 \geq \lambda_2 \geq \lambda_3 \geq \lambda_4$, then the concurrence is $C_{i,j} = \max(\sqrt{\lambda_1} - \sqrt{\lambda_2} - \sqrt{\lambda_3} - \sqrt{\lambda_4}, 0)$. Due to the conservation of magnetization, the concurrence in the

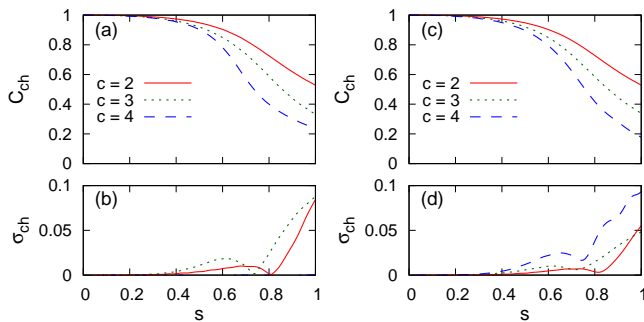


FIG. 5. Time dependence of the average C_{ch} [(a) and (c)] and the standard deviation σ_{ch} [(b) and (d)] of the intra-chain concurrence for several values of connectivity c of regular random graphs. The number of nodes are $N = 6$ [(a) and (b)] and $N = 8$ [(c) and (d)].

systems considered here has a simple form [25, 40]:

$$C_{i,j} = 2 \max(|z| - \sqrt{xy}, 0), \quad (13)$$

where $z = \langle \uparrow\downarrow | \rho_{ij} | \downarrow\uparrow \rangle$, $x = \langle \uparrow\uparrow | \rho_{ij} | \uparrow\uparrow \rangle$, and $y = \langle \downarrow\downarrow | \rho_{ij} | \downarrow\downarrow \rangle$.

The time dependence of the one-chain EE shown in the previous section implies that focusing on one chain is the key to find the relation between entanglement and MBL. We here introduce intra-chain concurrence, which is the concurrence in two spins in the same chain, and compare it with the concurrence in a disordered tight-binding chain.

A. intra-chain concurrence

In our system, a spin has two indices, e.g., node i and color a . Let $C(i, a; j, b)$ denote the concurrence in spins (i, a) and (j, b) . We define intra-chain concurrence as

$$C_{\text{ch}} = \frac{1}{2N} \sum_{i=1}^N \sum_{a=1}^q C(i, a; i, a+1), \quad (14)$$

which is scaled so that $C_{\text{ch}} = 1$ at $s = 0$. Equation (14) expresses the average of the nearest-neighbor concurrence in each chain. We perform numerical simulations with the same parameter setting as in Sec. IV.

The time dependence of the intra-chain concurrence is demonstrated in Fig. 5. The average intra-chain concurrence decreases monotonically. The larger the connectivity c of regular random graphs, the smaller the average intra-chain concurrence. The decrease in the intra-chain concurrence implies the decay of the entanglement between neighboring spins. This is caused by effective local fields which increases with time. In contrast, the standard deviation σ_{ch} of intra-chain concurrence has peaks, which is similar to that of the one-chain EE. Peak positions in Figs. 5(b) and 5(d) are close to those in Figs. 4(b) and 4(d), which implies that these peaks also indicate the MBL transition.

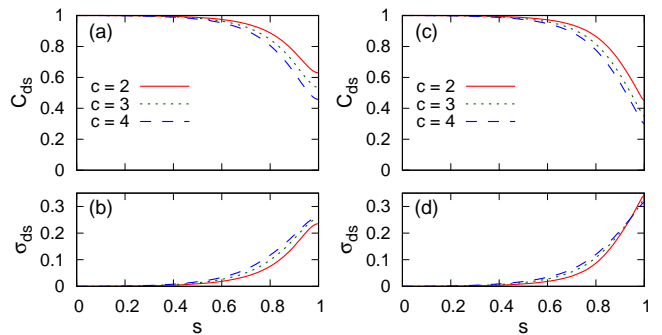


FIG. 6. Time dependence of the average C_{ds} [(a) and (c)] and the standard deviation σ_{ds} [(b) and (d)] of the disordered-chain concurrence for several values of parameter c which is related to disorder. The number of spins is $q = 4$, and the final time is $\tau = 20$ [(a) and (b)] and $\tau = 200$ [(c) and (d)].

B. disordered-chain concurrence

As mentioned earlier, the system considered has an analogy to disordered spin chains. Then, can similar peaks appear in the standard deviation of concurrence in a disordered spin chain? To answer the question, let us consider a disordered tight-binding chain whose problem and driving Hamiltonians are respectively given by

$$H_{\text{p}} = J \sum_{a=1}^q h_a c_a^\dagger c_a, \quad (15)$$

$$H_{\text{d}} = -2J \sum_{a=1}^q (c_a^\dagger c_{a+1} + c_{a+1}^\dagger c_a), \quad (16)$$

where h_a is a local random field, and c_a^\dagger and c_a are the creation and annihilation operators of a spinless fermion, respectively. Suppose that there is only one fermion in a chain. Instead of real random numbers with a uniform distribution, we take $h_a = mh^{\text{eff}}$, where h^{eff} is the effective field given in Sec. II. Integer m is given by $m = \sum_i m_i$ ($i = 1, \dots, c$), where $m_i = 1$ with a probability $1/q$ and $m_i = -1$ with a probability $1 - 1/q$. Disordered-chain concurrence is simply defined as

$$C_{\text{ds}} = \frac{1}{2} \sum_{a=1}^q C_{a,a+1}, \quad (17)$$

which is scaled so that $C_{\text{ds}} = 1$ at $s = 0$.

Figure 6 shows the time dependence of the disordered-chain concurrence. The behavior is different from that of Fig. 5. The average of disordered-chain concurrence decreases monotonically, and its standard deviation increases almost monotonically. No peak appears in the middle of an annealing process, which implies that the MBL transition does not occur in this system. Actually, Anderson localization, instead of MBL, occurs in a disordered tight-binding chain. Since no many-body interaction exists, MBL does not occur in the tight-binding chain.

VI. DISCUSSION AND CONCLUSIONS

In Figs. 4 and 5, each curve of the standard deviation of the one-chain EE and the intra-chain concurrence has a peak followed by a trough in the middle of a CQA process. After the trough, the standard deviation increases again. The second peak is characteristic of the entanglement evolution in our system. Actually, in the case of a one-dimensional disordered spin chain, the standard deviation of the half-chain EE has only one peak [27–30]. This peak corresponds to the first peak of our case and indicates the fluctuation associated with the MBL transition. In the late stage of a CQA process, the wavefunction is very close to the ground state of the problem Hamiltonian. Since the problem Hamiltonian represents a classical system, the second peak reflects the variation of effective random fields rather than quantum effects.

We have found the evidence of the MBL transition in a CQA process. The MBL transition corresponds to peaks of the standard deviation of the one-chain EE [Figs. 4(b)

and 4(d)] and the intra-chain concurrence [Figs. 5(b) and 5(d)]. In a CQA process, intra-chain connection decreases, and the strength of effective random fields increases. However, the increase in the field strength, i.e., disorder, is not sufficient to cause the MBL transition. This is evident from the fact that the standard deviation of the disordered-chain concurrence increases only monotonically [Figs. 6(b) and 6(d)]. The characteristic behavior of entanglement in our system, compared with that of the disordered-chain concurrence, suggests that the inter-chain interaction as well as effective fields is an essential factor for the MBL transition.

ACKNOWLEDGMENTS

This work is partially supported by JSPS KAKENHI Grant Number JP18K11333, and the research grant from the Inamori Foundation.

-
- [1] R. Jozsa and N. Linden, Proc. R. Soc. Lond. A **459**, 2011 (2003).
 - [2] G. Vidal, Phys. Rev. Lett. **91**, (2003).
 - [3] G. Vidal, Phys. Rev. Lett. **93**, (2004).
 - [4] R. Orús and J. I. Latorre, Phys. Rev. A **69**, 052308 (2004).
 - [5] P. Hauke, L. Bonnes, M. Heyl, and W. Lechner, Front. in Phys. **3**, (2015).
 - [6] J. Batle, C. H. R. Ooi, A. Farouk, M. Abutalib, and S. Abdalla, Quantum Inf. Process. **15**, 3081 (2016).
 - [7] T. Albash and D. A. Lidar, Rev. Mod. Phys. **90**, 015002 (2018).
 - [8] T. Kadowaki and H. Nishimori, Phys. Rev. E **58**, 5355 (1998).
 - [9] J. Brooke, D. Bitko, T. F. Rosenbaum, and G. Aeppli, Science **284**, 779 (1999).
 - [10] A. Das and B. K. Chakrabarti, Rev. Mod. Phys. **80**, 1061 (2008).
 - [11] E. Farhi, J. Goldstone, S. Gutmann, J. Lapan, A. Lundgren, and D. Preda, Science **292**, 472 (2001).
 - [12] R. Martoňák, G. E. Santoro, and E. Tosatti, Phys. Rev. E **70**, 057701 (2004).
 - [13] K. Kurihara, S. Tanaka, and S. Miyashita, in *Proceedings of the Twenty-Fifth Conference on Uncertainty in Artificial Intelligence*, UAI '09, 2009, pp. 321–328.
 - [14] B. Altshuler, H. Krovi, and J. Roland, Proc. Natl. Acad. Sci. U.S.A. **107**, 12446 (2010).
 - [15] O. Titiloye and A. Crispin, Discrete Optimization **8**, 376 (2011).
 - [16] O. Titiloye and A. Crispin, PLOS ONE **7**, e50060 (2012).
 - [17] J. M. Deutsch, Phys. Rev. A **43**, 2046 (1991).
 - [18] M. Srednicki, Phys. Rev. E **50**, 888 (1994).
 - [19] M. Rigol, V. Dunjko, and M. Olshanii, Nature (London) **452**, 854 (2008).
 - [20] M. Žnidarič, T. Prosen, and P. Prelovšek, Phys. Rev. B **77**, 064426 (2008).
 - [21] J. H. Bardarson, F. Pollmann, and J. E. Moore, Phys. Rev. Lett. **109**, 017202 (2012).
 - [22] M. Serbyn, Z. Papić, and D. A. Abanin, Phys. Rev. Lett. **110**, 260601 (2013).
 - [23] M. Serbyn, Z. Papić, and D. A. Abanin, Phys. Rev. Lett. **111**, 127201 (2013).
 - [24] S. Bera, H. Schomerus, F. Heidrich-Meisner, and J. H. Bardarson, Phys. Rev. Lett. **115**, 046603 (2015).
 - [25] S. Bera and A. Lakshminarayanan, Phys. Rev. B **93**, 134204 (2016).
 - [26] T. Enss, F. Andraschko, and J. Sirker, Phys. Rev. B **95**, 045121 (2017).
 - [27] D. J. Luitz, N. Laflorencie, and F. Alet, Phys. Rev. B **91**, 081103 (2015).
 - [28] V. Khemani, S. P. Lim, D. N. Sheng, and D. A. Huse, Phys. Rev. X **7**, 021013 (2017).
 - [29] V. Khemani, D. N. Sheng, and D. A. Huse, Phys. Rev. Lett. **119**, 075702 (2017).
 - [30] J. A. Kjäll, J. H. Bardarson, and F. Pollmann, Phys. Rev. Lett. **113**, (2014).
 - [31] K. Kudo, Phys. Rev. A **98**, 022301 (2018).
 - [32] I. Hen and F. M. Spedalieri, Phys. Rev. Applied **5**, 034007 (2016).
 - [33] I. Hen and M. S. Sarandy, Phys. Rev. A **93**, 062312 (2016).
 - [34] F. Gaitan and L. Clark, Phys. Rev. Lett. **108**, 010501 (2012).
 - [35] Z. Bian, F. Chudak, W. G. Macready, L. Clark, and F. Gaitan, Phys. Rev. Lett. **111**, 130505 (2013).
 - [36] F. Gaitan and L. Clark, Phys. Rev. A **89**, 022342 (2014).
 - [37] A. Lucas, Frontiers in Phys. **2**, 5 (2014).
 - [38] E. G. Rieffel, D. Venturelli, B. O’Gorman, M. B. Do, E. M. Prystay, and V. N. Smelyanskiy, Quantum Inf. Process. **14**, 1 (2015).
 - [39] D. N. Page, Phys. Rev. Lett. **71**, 1291 (1993).
 - [40] K. M. O’Connor and W. K. Wootters, Phys. Rev. A **63**, 052302 (2001).